https://doi.org/10.5194/acp-2022-667
Preprint. Discussion started: 7 November 2022

Atmospheric Chemistry and Physics Discussions

Measurement report: Radiative efficiency estimates of $(CF_3)_2CFCN$, CF_3OCFCF_2, and $CF_3OCF_2CF_3$ using high-resolution Fourier transform infrared spectroscopy

Beni Adi Trisna[1], Seungnam Park[2], Injun Park[3], Jeongsoon Lee[1], Jeong Sik Lim[1]

[1]Greenhouse Gas Metrology team, Korea Research Institute of Standard and Science (KRISS), Science of Measurement, University of Science and Technology (UST), Daejeon, 34113, Republic of Korea
[2]National Centre of Standard Reference Data (NCSRD), Korea Research Institute of Standard and Science (KRISS), Daejeon, 34113, Republic of Korea
[3]Interface Materials and Chemical Engineering Research Centre, Korea Research Institute of Chemical Technology (KRICT), Daejeon, 34114, Republic of Korea

Correspondence to: Jeongsoon Lee (leejs@kriss.re.kr) and Jeong Sik Lim (lim.jeongsik@kriss.re.kr)

Abstract. Absorption cross-sections (ACS) of emerging greenhouse gases (GHG) were measured to estimate the radiative efficiencies (RE) using high-resolution Fourier transform infrared spectroscopy (HR-FTIR). For quantitative spectroscopy, the Beer–Lambert parameters of absorber pressure, temperature, and optical pass length (OPL) have been accurately determined to be traceable to the primary standards. The OPL of the multipass cell (MP) mounted on the HR-FTIR spectrometer was spectroscopically calibrated. A ratio of the averaged N_2O absorptions was measured in the range of 2217.4–2219.0 cm^{-1} with a spectral resolution of 0.026 cm^{-1}, yielding a ratio of OPLs between the MP and reference cell (RC). This cell-to-cell comparison (CC) method does not include the uncertainty in the referring line strength, thereby reducing the calibration uncertainty compared with a direct line-strength referring method. With the OPL-calibrated MP (3.169 ± 0.079 m), the ACSs were measured at low absorber pressures with a spectral resolution of 2 cm^{-1}, integrated at 10 cm^{-1} intervals, and multiplied by the new narrow band model to yield the RE values. The RE values of the classic GHGs CF_4, SF_6, and NF_3 were evaluated to be 0.085 ± 0.002, 0.573 ± 0.016, and 0.195 ± 0.008 W m^{-2} ppb^{-1}, respectively, which are consistent with previously reported values. For the emerging GHGs, the RE values were determined to be 0.201 ± 0.008 $Wm^{-2}ppb^{-1}$ for $(CF_3)_2CFCN$ (heptafluoroisobutyronitrile, commercially referred to as *Novec-4710*), 0.328 ± 0.013 $Wm^{-2}ppb^{-1}$ for CF_3OCFCF_2 (perfluoro methyl vinyl ether, PMVE), and 0.544 ± 0.022 $Wm^{-2}ppb^{-1}$ for $CF_3OCF_2CF_3$ (1,1,1,2,2-pentafluoro-2-(trifluoromethoxy)ethane, PFMEE).

1 Introduction

Radiative efficiency (RE) enables the quantification of variations in radiative forcing (RF), which is the change in thermal energy flux in the atmosphere caused by a change in the unit concentration of a single greenhouse gas (GHG). Emitted GHGs undergo degradation via a range of atmospheric reactions that define their atmospheric lifetimes (AL). The pulsed 'unit emission' of a GHG exhibits a timely reduction in the incoming thermal energy flux based on the AL. Integrating the RE-adjusted time-varying RF in a designated time horizon yields the global warming potential (GWP). In the Nationally Determined Contribution (NDC), GHG emissions are reported in terms of the CO_2-equivalent amount as rated by the GWP,

https://doi.org/10.5194/acp-2022-667
Preprint. Discussion started: 7 November 2022

Atmospheric Chemistry and Physics Discussions

with the value for CO_2 designated as 1 (Paris Agreement, 2015). To date, the GWPs of major GHGs have been reported in the IPCC 6th assessment report (AR6) by combining multiple RF and AL values obtained from different independent studies (IPCC, 2021). Although the GWP is the *de facto* climate metric standard for reporting in the NDC, there has been debate within the climate research community regarding the reliability of GWP values (Denison et al., 2019; Rosenzweig et al., 2018). The climate impacts of emission pathways can be misinterpreted by the simple aggregation of GWPs of different GHGs. To resolve this problem, alternative climate metrics, such as the global temperature change potential, and short-lived climate pollutants adjusted GWP have been suggested to fill the error gap in the prediction of target atmospheric temperatures in the characterization of the mitigation pathways (Allen et al., 2018; Denison et al., 2019; Lynch et al., 2020). Therefore, as a means of eliminating the intrinsic error in the GWP assessment, the uncertainty in the GWP measurement has gained increasing attention. The IPCC AR6 includes a discussion regarding the major uncertainty sources of climate metrics that originate from the AL, RE, chemical response, and absolute GWP of CO_2 (IPCC, 2021). Andersen et al. (2021) have recently pointed out that a standardization of laboratory kinetics measurements is required to enhance the reliability of AL measurements. Similarly, the reliability of the RE values can be enhanced by the accurate measurement of the absorption cross-section (ACS), which is an in-laboratory measurement parameter for RE. According to the IPCC AR6, RE uncertainties are generally the major contributors to the total uncertainty in the GWP, with proportions of up to 22%, depending on the compound (IPCC, 2021). In this study, we propose an accurate measurement method for the RE and assess the uncertainty budget in detail.

The classic and emerging GHGs were comprehensively evaluated as follows: (1) The spectroscopic calibration of the optical path length (OPL) was carried out using high-resolution Fourier transform infrared spectroscopy, an essential tool for accurate ACS measurements. (2) The new narrow band model (nNBM), wherein the stratospheric-temperature adjustment has been applied to the NBM model, was used to evaluate the RE value. (3) An uncertainty assessment of the RE values of the classic and emerging GHGs was conducted. The emerging GHGs for which the RE values were assessed in this study were heptafluoro-isobutyronitrile (commercially known as *Novec*-4710, $(CF_3)_2CFCN$), 1,1,1,2,2-pentafluoro-2-(trifluoromethoxy)ethane (PFMEE, $CF_3OCF_2CF_3$), and perfluoro methyl vinyl ether (PMVE, CF_3OCFCF_2). *Novec*-4710 is used as an alternative to SF_6 as an insulator for gas insulated switchgear (GIS) (Andersen et al., 2017; Laruelle et al., 2017; Zhao et al., 2019). PMVE and PFMEE are considered as future alternatives to chlorofluorocarbons (CFCs), although their RE values have been rarely reported to date (Kim et al., 2014; Li et al., 2000). The values obtained for the classic GHGs (NF_3, SF_6, and CF_4) were compared with those reported in previous studies to corroborate the validity of the proposed method.

2 Methods

2.1 Instrumental setup

High-resolution Fourier transform infrared spectrometer (HR-FTIR, Bruker IFS 125HR) dedicated entire measurement procedure. The spectrometer was equipped with a KBr beam splitter, which enabled measurements between 400 and 6500 cm^{-1}. The measurements were conducted by passing a collimated thermal light source (Globar) through a reference gas cell (RC)

https://doi.org/10.5194/acp-2022-667
Preprint. Discussion started: 7 November 2022

Atmospheric Chemistry and Physics Discussions

or a White-type multipass cell (MP). A mercury cadmium telluride (MCT) detector, cooled using liquid nitrogen, was used for all the spectroscopic calibration measurements of the OPLs and ACSs of the target GHGs. For the MCT detector, a nonlinearity correction was applied to the detector response when recording the interferograms. The OPUS software implemented the correction algorithm for the instrumental control and spectrum acquisition. For the spectroscopic calibration of the OPL, N_2O absorption spectra were obtained at a resolution of 0.026 cm^{-1} from the RC and MP (maximum OPD = 36 cm). The instrumental line shape (ILS) was retrieved from the measured N_2O spectra in the RC using the LINEFIT program (Fig. S1). Inverse modelling of the modulation efficiency (ME) and phase error (PE) in the domain of the optical path difference (OPD) was performed (Hase et al., 1999). The pure absorption spectrum of N_2O was forward-modelled using the Voight profile with the HITRAN parameters, such as line strength and self-broadening coefficient. The residuals between the measured and modelled spectra were minimized to provide the best fits of the ME and PE values as a function of the OPD. The ILS was then reconstructed using the preset apodization function of the Norton–Beer strong. Subsequently, the N_2O spectra in the MC was obtained utilizing the same instrumental parameters as used for the RC measurement. The ratio of the absorption areas between the MP and RC was obtained via the deconvolution of the ILS (Fig. 1).

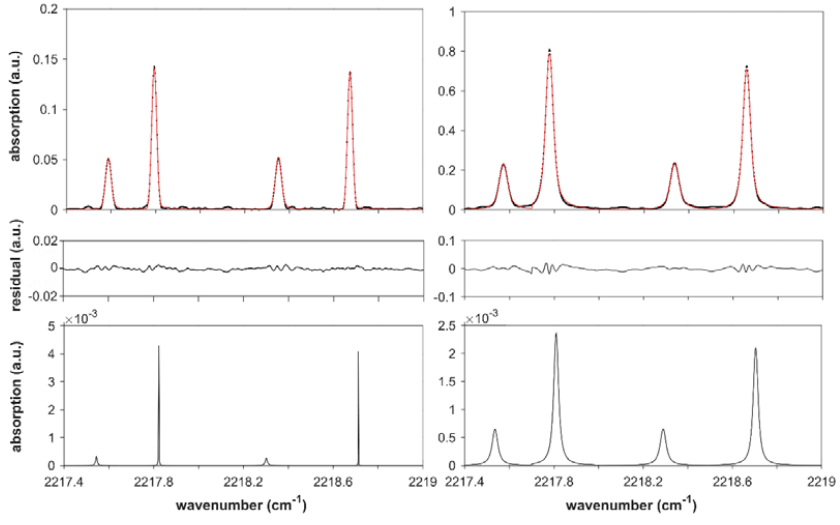

Figure 1. Instrumental line shape (ILS)-convoluted Voight fit of the measured spectrum of the reference absorption cell (left image in the upper row). ILS-convoluted Voight fit of the measured spectrum of the multipass absorption cell (right image in the upper row). The residuals of each fit are shown in the middle row of the graph. The lower row shows ILS-deconvoluted spectra of the reference and multipass cells. The areas under the ILS-deconvoluted spectra are compared, and the optical path length (OPL) of the multipass absorption cell is determined using Eq. (4). The areas for the reference and multipass cells are 2.9×10^{-5} and 2.2×10^{-4}, respectively, resulting in an OPL of the MC of 3.169 ± 0.079 m.

If the ILS was not deconvoluted, the ratio value would be considerably distorted from the original value owing to the differing extents of pressure broadening. The OPL of the MC was then determined by a comparison with the peak area of the RC measurement. For this comparison, the absorption lines of N_2O were selected from 2217.4 cm^{-1} to 2219.0 cm^{-1}. The theoretical details of the OPL calibration method are presented in the supporting information. The total pressures of the RC and MP were 0.71 and 70.93 Torr, respectively. To obtain the values lying within the linear region of the curve-of-growth (COG), the

https://doi.org/10.5194/acp-2022-667
Preprint. Discussion started: 7 November 2022

Atmospheric Chemistry and Physics Discussions

concentration of N_2O in the MC was diluted to 481.943 μmol mol^{-1} using an N_2 broadener, which corresponds to an absorption burden (OPL × partial pressure) of 10.6 cm Torr (Fig. 2). A detailed discussion of the COG analysis is also provided in the supporting information. The length between the inner faces of the RC (20.01 ± 0.05 mm (1σ)) is traceable to the national gauge block standards. Given that the cell temperature (297 ± 1 K) was well equilibrated to that of the surroundings, it can be assumed that the temperature distribution of the gas was homogeneous throughout the beam path. The spectra were averaged 64 times.

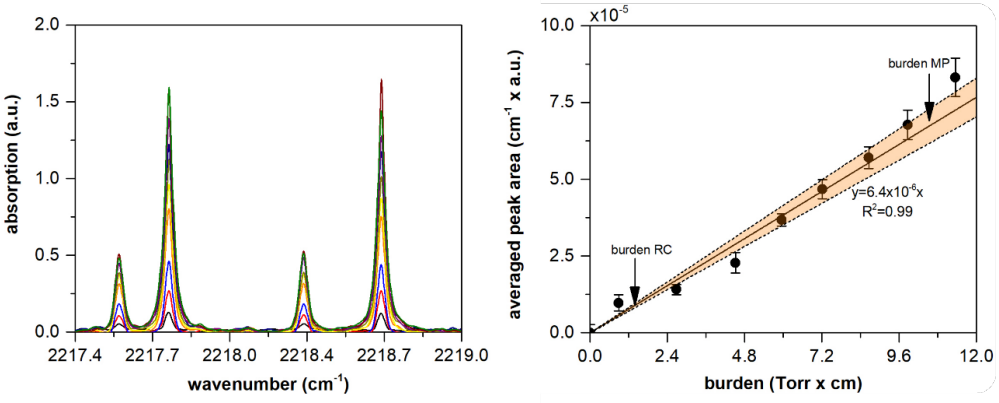

Figure 2. Absorption of N_2O with respect to cell pressure (left). The curve-of-growth (COG) plot for the corresponding peaks (right). Averaged peak areas after ILS deconvolution are shown with respect to the absorption burden (pressure × OPL). Without ILS deconvolution, no linearity of fit was obtained. A weighted least squares method was employed to fit the measured dataset with a straight line crossing the origin. The orange areas represent the confidence bands (at k = 2) of the fitted line. The COG analysis shows that the OPL calibration was valid for the cell-to-cell comparison (CC) method by occurring within the linear region of the COG.

The ACSs were obtained by averaging 256 spectra at a spectral resolution of 2 cm^{-1}, measured within the wavenumber range of 500–3000 cm^{-1}. To get low absorption burdens at the nominal OPL of the MP, the gases to be measured were gravimetrically diluted to a designated concentration with an N_2 broadener (the typical gravimetric uncertainty is below 1.5%). This was also required to ensure the accuracy of the pressure readings for trace levels of the absorbing gas (< 0.1 Torr) using pressure gauges, the full scales of which are over 100 Torr (accuracy 0.05 Torr) with a valid dynamic range of 0% to 95% (Johnson et al., 2021). The overall signal-to-noise ratios (S/N) of the absorption spectra were higher than 2000. NF_3 at a pressure of 0.035 Torr was mixed with N_2 to yield a total pressure of 354.97 Torr in the MP. In brief, the partial pressures for SF_6, CF_4, PMVE, and PFMEE were 0.0057, 0.021, 0.047, and 0.039 Torr, respectively, using N_2 as the broadening agent. For *Novec*-4710, the partial pressure was set at 0.11 Torr and broadened using CO_2. The pressure gauges (INFICON, CDG025D and MKS, 626A13TBE) were calibrated against the KRISS standards. The temperature sensors (Testek, 303A and SK Sato, PC-5000TRH-II) were calibrated against a platinum resistance thermometer (Fluke-Hart Scientific, 5628) that was traceable to the NIST temperature fixed-point standards. The other instrumental parameters for the OPL calibration and ACS measurements are listed in Table 1.

https://doi.org/10.5194/acp-2022-667
Preprint. Discussion started: 7 November 2022

Atmospheric Chemistry and Physics Discussions

120

Table 1. Instrumental setup and experimental conditions

Parameter	OPL calibration		ACS Measurement
	RC (N_2O)	MP (N_2O)	
Spectral range measured	6500–500 cm^{-1}	6500–500 cm^{-1}	6500–500 cm^{-1}
Spectral resolution	0.025 cm^{-1}	0.025 cm^{-1}	2 cm^{-1}
Light source	SiC Globar	SiC Globar	SiC Globar
Collimator focal length	418 mm	418 mm	418 mm
Optical speed	*f*/6.5	*f*/6.5	*f*/6.5
Beam splitter	KBr	KBr	KBr
Detector	LN_2-cooled MCT	LN_2-cooled MCT	LN_2-cooled MCT
Gas cell	Glass Single-pass Sealed Cell 20.01 mm	Glass Multi-pass cell 3100 mm (max. 28,000 mm)	Glass Multi-pass cell 3100 mm (max. 28,000 mm)
Optical path length	20.01 mm	3100 mm	3100 mm
Mirror velocity	60 kHz	60 kHz	60 kHz
Acquisition mode	Single-sided, Forward-Backward	Single-sided, Forward-Backward	Single-eided, Forward-Backward
Jacquinot aperture	2 mm	2 mm	4 mm
Laser wavenumber	15,798.015 cm^{-1}	15,798.015 cm^{-1}	15,798.015 cm^{-1}
Number scan sample	64	64	256
High-pass filter	Open	Open	Open
Low-pass filter	20 kHz	20 kHz	20 kHz
Preamplifier gain	2 kHz	2 kHz	2 kHz
Switch gain	n/a	n/a	n/a
High freq. limit	15,798	15,798	15,798
Low freq. limit	0	0	0
Phase resolution	2 cm^{-1}	2 cm^{-1}	2 cm^{-1}
Phase correction	Mertz	Mertz	Mertz
Apodization mode	Norton–Beer, Strong	Norton–Beer, Strong	Boxcar
Zero filling factor	8	8	32
Pressure gauge	n/a	MKS 626A	INFICON CDG025D and MKS 626A
Partial (total) pressures	0.7 Torr (0.7 Torr)	0.034 Torr (70.93 Torr)	See main text
Burdens (pressure × OPL)	1.4 cm·Torr	10.6 cm·Torr	See main text

https://doi.org/10.5194/acp-2022-667
Preprint. Discussion started: 7 November 2022

Atmospheric Chemistry and Physics Discussions

2.2 Spectroscopic calibration method for the optical path length

The quantification of gas absorption requires the Beer–Lambert parameters, such as pressure, temperature, and OPL. In this study, the pressures and temperatures were measured directly. The OPL of MP was calibrated based on HR-FTIR spectroscopy, and its uncertainty was assessed directly. The absorbance measured at high pressures exhibited a different extent of saturation effect according to respective bands, disobeying the linear property of the Beer–Lambert law (Johnson et al., 2021). Therefore, it was critical to use the MP at low partial pressures. However, it has been common to use a single pass cell with a (sometimes mechanically determined) preassigned OPL uncertainty or only the nominal OPL value (Harrison et al., 2010; Harrison, 2015; Harrison, 2020; Robson et al., 2006). However, measuring the OPL of an MP requires an alternative approach rather than the mechanical method for the OPL of a single pass cell. In this regard, Nwaboh et.al. demonstrated a calibration method for the OPL of an MP using tunable diode laser absorption spectroscopy (TDLAS), in which the OPL and absorption are related as follows (Nwaboh et al., 2014):

$$x_{abs} = \frac{k_B \cdot T}{S_T \cdot L \cdot P_{abs}} \cdot A_{abs}, \quad (1)$$

where x_{abs} is amount fractions of absorber, k_B is the Boltzmann constant, T is the temperature, S_T is the line strength of the probed absorption line, r_{iso} is the isotope abundance of N_2O, L is OPL, P_{abs} is the partial pressure of the absorbing gas, and A_{abs} is the integrated peak area under the absorption line of the absorbing gas ($\int_{-\infty}^{\infty} A_{meas}(\tilde{\nu} - \tilde{\nu}_0)d\tilde{\nu}$), where $\tilde{\nu}_0$ is the center transition wavenumber. Using Eq. (1), L_{MP} can be obtained directly by comparing the referred line strength, hereafter referred to as the direct line-strength referring (DLR) method. Nwaboh et al. reported the OPL calibration result of the absorption cell against a line strength of CH_4 as 4987.3 cm^{-1} ((8.289 ± 0.414) × 10^{-22} cm^{-1} / (cm^{-2} mol C)), and 95.4% contribution to the standard uncertainty of OPL, which led to a relative standard uncertainty of 5% (Nwaboh et al., 2014). A similar phenomenon has been reported in the calibration of gas concentrations (x_{abs}) using cavity ringdown spectroscopy (CRDS), wherein the expected value of the OPL was substituted by the direct measurement of the ringdown time. Consequently, the calibration of x_{abs} against S_T in the CRDS measurements is analogous to the OPL calibration in the TDLAS measurement. The uncertainty in S_T contributed over 80% to the standard uncertainty in x_{abs}, which was 1.2% of the calibrated value (Kim et al., 2021). The findings of these studies implied that the DLR method needs to be bypassed to avoid the direct use of the line strength, which in classic line databases, such as HITRAN and GEISA, exhibits a non-negligible or considerably high uncertainty. Instead, we attempted to construct a measurement traceability chain of the OPL of the MP L_{MP} to the national gauge block using the cell-to-cell comparison (CC) method. In the CC method, line strength plays the role of a mediator between the measurements of the RC and MP (Nwaboh et al., 2014). The uncertainty of OPL of RC L_{RC} (0.12%, including the measurement uncertainty using callipers) was better than that of the referred line strengths. Although experimentally determined uncertainties of the referred N_2O lines in this study, (0111) ← (0110) R9e (first peak), (0001) ← (0000) P7e (second peak), (0111) ← (0110) R10e

https://doi.org/10.5194/acp-2022-667
Preprint. Discussion started: 7 November 2022

Atmospheric Chemistry and Physics Discussions

(third peak), and (0001) ← (0000) P6e (the fourth peak), have not been reported (Table S3), those of N_2O have typically been reported to be between 2% and 5% within the measurement range of 0–3000 cm^{-1}(Gordon et al., 2017; Pinnock and Shine, 1998). Notably, other candidates, such as CO_2 and CH_4, have exhibited similar levels of uncertainty. As discussed in Sect. 3.1, the uncertainties of the referred line strengths were not required in the uncertainty evaluation process.

An optical bandpass filter (OBF) at a central wavelength of 4.5 μm was used to measure the spectra obtained from the RC. The OBF in front of the RC enabled to set similar radiant powers transmitted through both the MP and RC, because the throughput of the MP was reduced to 80% owing to the surface aging of the gold reflection mirrors. This ensured that the interferograms of the RC and MP were obtained at the same aperture size of 2 mm and at similar S/N levels. The identical field-of-view function (same aperture size) between multiple measurements was required to ensure identical ILSs for the comparison of the MP and RC measurements (Smith et al., 2011). We assumed that there was no significant drift in the ILS during the entire measurement process. The boxcar apodization function should yield a sharper ILS looking similar to the sinc function at the set maximum OPD. However, the Norton–Beer strong function provides a reasonable symmetric line shape by effectively suppressing the sideband even at a less ideal alignment status of the interferometer.

The spectral absorption $A(\tilde{\nu})$ was calculated as $-\ln(\Phi(\tilde{\nu})/\Phi_0(\tilde{\nu}))$, where $\Phi(\tilde{\nu})$ and $\Phi_0(\tilde{\nu})$ are the transmitted and incident radiant powers, respectively. The measured spectral absorbance at the transition wavenumber $\tilde{\nu}_0$, $A_{meas}(\tilde{\nu})$, can be expressed by the convolution of the pure gas absorption line $A_{pgs}(\tilde{\nu})$ and the ILS as follows:

$$A_{meas}(\tilde{\nu}) = A_{pgs}(\tilde{\nu}) \otimes ILS(\tilde{\nu}) \quad (2)$$

Therefore, in FTIR spectroscopy, A_{abs} is the integrated area under the ILS-deconvoluted absorption line of the absorbing gas, namely, $\int_{-\infty}^{\infty} A_{pgs}(\tilde{\nu} - \tilde{\nu}_0)d\tilde{\nu}$. In contrast, using TDLAS, an ILS of less than a few megahertz could be treated as a delta function because the linewidths of the well-separated absorption lines of a small molecule are typically over a few gigahertz. This aspect of laser-based measurements simplifies the procedure of OPL calibration, which is facilitated by the direct measurements of the RC and MP without the retrieval of the pure gas spectra. Because the linewidth of the FTIR ILS obtained in the present study was comparable to that of the pure gas absorption line, the peak area measured using FTIR spectroscopy was significantly distorted from that of the pure gas absorption line. Mathematically, for a comparison of the integrated area, the convoluted functions of the numerator and denominator cannot be cancelled ($\frac{\int a(x)}{\int b(x)} \neq \frac{\int a(x) \otimes c(x)}{\int b(x) \otimes c(x)}$). Based on Eq. (1), L_{MP} was obtained by comparing the spectral absorptions of the RC and MP and is expressed as follows:

$$L_{MP} = \frac{T_{MP} \cdot P_{RC} \cdot L_{RC} \cdot A_{MP} \cdot S_{T,RC}}{T_{RC} \cdot P_{MP} \cdot A_{RC} \cdot S_{T,MP}} \quad (3)$$

https://doi.org/10.5194/acp-2022-667
Preprint. Discussion started: 7 November 2022


Atmospheric Chemistry and Physics Discussions

S_T comprises the temperature-dependent prefactor (P_T) and reference line strength (S_0), as described in the supporting information (ST 3). The peak areas of the pure gas spectra of the MP and RC (A_{MP} and A_{RC}, respectively) were estimated using the trapezoidal method. These peak areas fell within the linear region of the COG plot, ensuring the accuracy of this calibration method by securing linearity (Fig 2). However, the uncertainty of the slope of the COG plot should also be included in the uncertainty of A_{MP} (ST 2). The partial pressure of the broadener was not a factor in determining the values of A_{MP} and A_{RC}.

2.3 Estimation of radiative efficiency

RE is a measure of the RF for a unit change in the atmospheric concentration of a gas, generally reported in units of W m^{-2} ppb^{-1}. To obtain the RE values, the ACS of a GHG is multiplied by the RF as follows:

$$RE = \sum_{i=1}^{250} RF_i \cdot \sigma_i(\tilde{\nu}, P_{abs}, T), \quad (4)$$

where RF_i is the applied RF model and $\sigma_i(\tilde{\nu}, P_{abs}, T)$ is the integrated ACS (iACS) at the i-th wavenumber block. The instantaneous radiative forcing (IRF) model, which accounts for the global and annual means of the Earth's atmosphere, was proposed by Pinnock et al. (1995). The Pinnock curve is based on a 10 cm^{-1} narrow-band model (NBM). Hodnebrog et al. (2013) subsequently updated the Pinnock curve by increasing the spectral resolution from 10 to 1 cm^{-1} using the Oslo line-by-line (OLBL) radiative transfer code at a spectral resolution of 0.02 cm^{-1}, which is hereafter referred to as high-resolution NBM (hNBM). Although the OLBL model includes an improved representation of the water vapor continuum and some changes to the representation of clouds, it is computationally expensive to introduce the necessity of a parameterized RF model such as an NBM (Hodneborg et al., 2020; Shine and Myhre, 2020). In the narrow-band model (nNBM) proposed by Hodnebrog et al. (2020), the effect of the stratospheric temperature adjustment was added to the NBM. Notably, in the studies conducted by Hodnebrog et al., a lifetime correction for short-lived species was applied to improve the breakdown of the baseline assumption, which accounts for the well-mixed condition of a stable GHG within the atmosphere. In the present study, we applied the nNBM model without the lifetime correction. σ_i is the integrated ACS (iACS) that is obtained at a spectral resolution of 2 cm^{-1} and integrated at a 10 cm^{-1} block interval. We did not observe any dependence of the RE values on the spectral resolution of ACS, which tends to imply a negligible effect of the variation in the linewidth of the ILS on the value of iACS. Johnson et al. demonstrated that the iACS of isobutane measured at multiple resolutions between 0.01 and 4.0 cm^{-1} were in good agreement, thereby implying that resolution dependence did not need to be considered (Johnson et al., 2021). Consequently, RE is indeed an iACS that is weighted by an RF model from 0 to 3000 cm^{-1}. Above 3000 cm^{-1}, solar radiation is strongly reduced in the atmosphere, thus indicating that laboratory-measured ACS values exceeding 3000 cm^{-1} do not influence the RE values (Pinnock et al., 1995); $\sigma_i(\tilde{\nu}, P_{abs}, T)$ is expressed as follows (Harrison et al., 2010; Harrison, 2015; Harrison, 2020):

https://doi.org/10.5194/acp-2022-667
Preprint. Discussion started: 7 November 2022

Atmospheric Chemistry and Physics Discussions

$$\sigma_i(\tilde{\nu}, P_{abs}, T) = \frac{10^4 \cdot k_B \cdot T}{L_{MP} \cdot P_{abs}} \ln\left(\frac{\Phi_{0,i}(\tilde{\nu})}{\Phi_i(\tilde{\nu}, P_{abs}, T)}\right) \quad (5)$$

ACS is expressed in terms of cm^2 molecule^{-1}. Due to instrumental limitations, we did not measure ACSs below 500 cm^{-1} in the present study, which may have introduced additional uncertainty in the RE value for cases in which these absorption bands occur (Hodnebrog et al., 2013).

3 Results and Discussion

3.1 Calibration of optical path length

Figure 2 shows the measurement results of the spectroscopic calibration of L_{MP}. According to Eq. (3), the ratio of A_{MP} to A_{RC} results in L_{MP} at a given pressure and temperature. In our study, four absorption lines from 2217.4 to 2219.0 cm^{-1} were simultaneously fitted to minimize the fit residuals. In this 'multispectra fitting' method, each peak was modelled using the Voight profiles with a fixed Doppler width (g_D), independent Lorentzian widths (g_L), and peak areas (A_{abs}). This is because the Doppler width depends only on the temperature and molecular weight, which are universal for every absorption line. In contrast, g_L and A_{abs} are inherent parameters of each absorption line. In every optimization step, the retrieved ILS $ILS(\tilde{\nu})$ was convoluted to the modelled pure gas spectrum $A_{pgs}(\tilde{\nu})$, and the residuals between the measured and modelled spectra were minimized to obtain the best fit for the spectral parameters (A_{abs}, g_L, g_D). The measurement of the pressure broadening coefficient was beyond the scope of this study because the peak area was not affected by pressure broadening. Because the temperature variations in the MP and RC during the experiments are independent of each other, the uncertainties in $S_{T,RC}$ and $S_{T,MP}$ should be independently determined (ST 3). The combined standard uncertainty in L_{MP} was estimated based on the general law of uncertainty propagation and the derivation of Eq. (3) as follows (JCGM, 2008):

$$ru^2(L_{MP}) = ru^2(A_{MP}) + ru^2(A_{RC}) + ru^2(P_{T,MP}) + ru^2(P_{T,RC}) + ru^2(L_{RC}) + ru^2(T_{MP}) + ru^2(T_{RC}) + ru^2(P_{MP}) + ru^2(P_{RC}), \quad (6)$$

where *ru* is the relative uncertainty. An advantage of the CC method is indicated in Eq. (6). Because the S_0 values of $S_{T,RC}$ and $S_{T,MP}$ are fully correlated (ρ = 1), $u(S_0)$ is cancelled by the negative definite covariance, namely $u^2(S_0) + u^2(S_0) - 2 \cdot cov(S_0, S_0) = 0$ (details are provided in ST 2) (Nwaboh et al., 2014). This approach is identical to the uncertainty assessment method applied in isotope dilution mass spectrometry (Pagliano and Meija, 2016). To determine the uncertainty in the P_T and $u(P_T)$, the thermodynamic (partition function and Boltzmann population) and quantum chemical (energy level) properties were weighted by the temperature. Details regarding the uncertainty evaluation method used for each term are described in the supporting information. In brief, the most sensitive sources of the OPL uncertainty were the absorption peak areas and L_{RC}, whereas the contributions by L_{MP} were similar to those of the other uncertainty sources, such as the temperature and pressure

https://doi.org/10.5194/acp-2022-667
Preprint. Discussion started: 7 November 2022

Atmospheric Chemistry and Physics Discussions

variations. The uncertainties of the absorption peak areas could be assigned to the instrumental origin. As shown in Fig. 1, clear undulating patterns in the fit residuals imply that the S/N ratio was sufficiently high to eliminate the white noise generated by the MCT detector. However, the undulations in the fit residuals (0.10% for MP and 0.13% for RC) were caused by the non-ideal ILS. An uneven sampling period, i.e. PE, and transversal displacement of the retroreflector, i.e. ME, during interferogram acquisition, both leading to a non-ideal ILS, are deemed to be critical factors affecting the fit residuals, considering that the Voight profile fits the absorption lineshape of N_2O especially well in the measured wavenumber range (Loos et al., 2015). It is also noted that the uncertainty of the slope of the curve-of-growth plot, $u(COG_{slope})$, was added to the uncertainty of A_{MP} to account for the comparability between the distinct values of L_{MP} and L_{RC}. The $u(COG_{slope})$ was found to contribute to up to 80% of $u(L_{MP})$. The slope of the COG plot was determined using the weighted least squares method with a straight line that crosses the origin. Consequently, we obtained the values of 3.169 ± 0.079 m for L_{MP}. The associated uncertainty budget is presented in Table S1.

3.2 Radiative efficiencies and associated uncertainties of emerging GHGs

Figure 3 shows the ACSs of the emitted GHGs. The uncertainty in the RE could be evaluated based on the law of uncertainty propagation from the derivation of Eq. (5) (JCGM, 2008). Assuming that all the uncertainty components are independent, the relative uncertainty in the RE, $ru(RE)$, can be estimated as follows:

$$ru^2(RE) = ru^2(L_{MP}) + ru^2(P) + ru^2(x) + ru^2(T) + 2 \cdot ru^2(rd) \quad (7)$$

where $ru(L_{MP})$, $ru(rd)$, $ru(P)$, and $ru(T)$ are the relative uncertainties of the L_{MP}, responsivity drift, total pressure measurement, and temperature variability, respectively. These uncertainty components were evaluated in the same manner as described in Sect. 3.1. Finally, $ru(x)$ is the uncertainty of the amount fraction of the absorbing gas. The partial pressure of the absorber is $P \times x$. Although the IR band shape generally varies depending on the temperature, the iACS might remain constant within the measured temperature range, leading $\Phi_i(\tilde{\nu}, P_{abs})$ (Harrison et al., 2020; Nelson et al., 2012). Therefore, the temperature terms in Eq. (5) exhibited dependence only on the prefactor. We did not consider the uncertainty of nNBM because the values were not reported in the previous study. A hidden uncertainty source may be the lack of data for bands below 500 cm^{-1} in the present study. For example, the missing bands in the far IR region may cause a systematic bias in the RE value, because low-frequency bending vibrations are present in larger compounds (Bravo et al., 2010).

https://doi.org/10.5194/acp-2022-667
Preprint. Discussion started: 7 November 2022

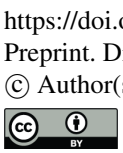

Atmospheric Chemistry and Physics Discussions

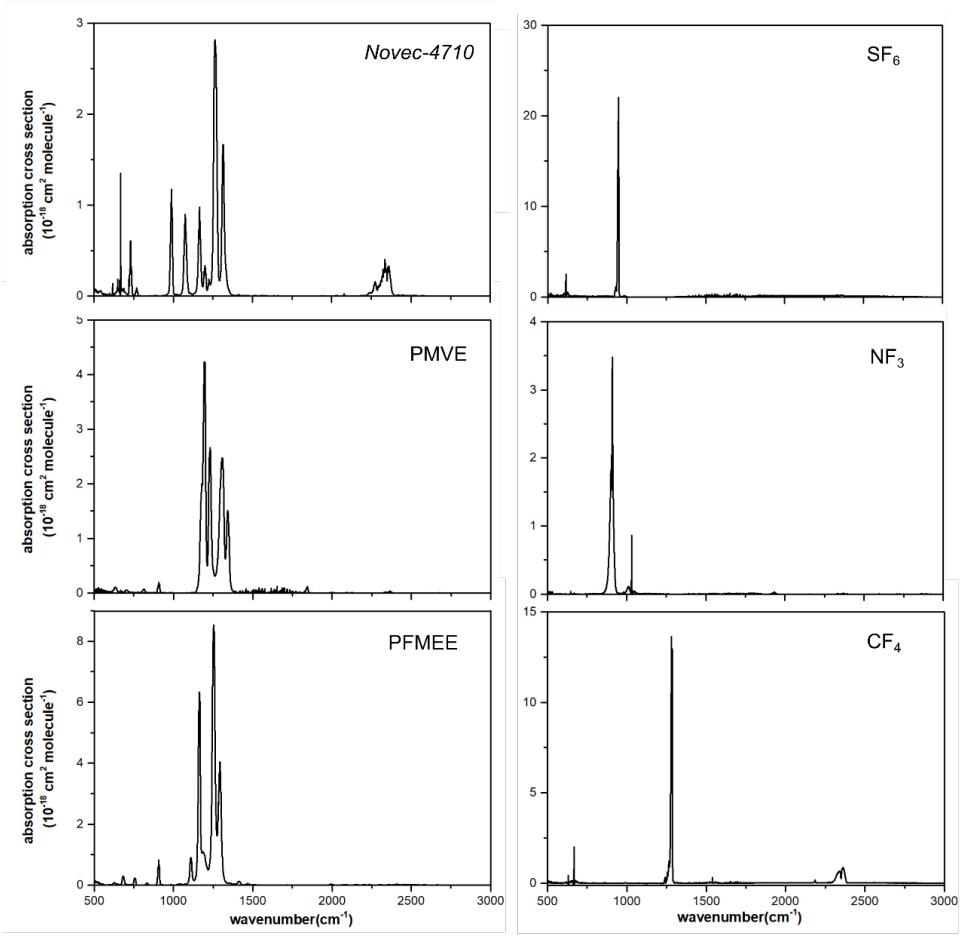

Figure 3. Absorption cross-section measurements for estimating the radiative efficiencies of *Novec-4710* at 297.15 ± 1 K, PMVE at 297.15 ± 1 K, PFMEE at 295.15 ± 1 K, SF_6 at 297.15 ± 1 K, NF_3 at 296.15 ± 1 K, and CF_4 at 296.15 ± 1 K.

3.2.1 Classic GHGs

The RE values of SF_6, CF_4, and NF_3 were revised using the proposed method, with absorption burdens of 1.8, 6.6, and 11.2 cm Torr, respectively. Numerous studies have reported the RE values of GHGs obtained using different RF models. In Hodnebrog et al. (2013), the RE values of SF_6 were summarized to be within the range of 0.49–0.68 W m^{-2} ppb^{-1}, depending on the RF model used (with a mean value of 0.56 W m^{-2} ppb^{-1}) (Hodnebrog et al., 2013). In the same study, the authors used hNBM with the lifetime correction to obtain an RE estimate of 0.57 W m^{-2} ppb^{-1}, which is consistent with the value obtained in the present study (0.573 ± 0.02 W m^{-2} ppb^{-1}) using the nNBM. In another study by Hodnebrog et al. (2020), the RE value with the nNBM and lifetime correction was also 0.57 W m^{-2} ppb^{-1}, which is consistent with that obtained in the current study. Although the value obtained in the present study was not lifetime-corrected, this consistency between studies would validate our proposed method, considering that lifetime corrections for long-lived GHGs is generally considered ineffective, owing to

https://doi.org/10.5194/acp-2022-667
Preprint. Discussion started: 7 November 2022

Atmospheric Chemistry and Physics Discussions

their long AL (e.g. 3,200 years for SF_6) facilitating a well-mixed condition within the atmosphere. The IPCC AR6 adopted a RE value of 0.567 W m^{-2} for SF_6, which is also in good agreement with the present study (IPCC, 2021). Similar relationships were identified for NF_3 and CF_4, which have long lifetimes of 740 and 50,000 years, respectively. (Table 2) However, the RE value of SF_6 reported by Jain et al., who used the NBM model, showed a considerable decrease compared with the values of SF_6, NF_3, and CF_4 obtained in other studies (Jain et al., 2000). In practice, the RF intensity in the 700–1000 cm^{-1} range of NBM is decreased in comparison with that of nNBM (Shine et al., 2020). In the same region, a strong band of SF_6 spikes, which might contribute to the considerable decrease in the NBM-based RE value of SF_6. Detailed uncertainty budgets for SF_6, NF_3, and CF_4 are presented in Tables S3, S4, and S5, respectively.

Table 2. Summary of the radiative efficiency values obtained in this study and previous studies. The confidence level used for RE uncertainty in this study is 95 %.

	Radiative efficiency ($Wm^{-2}ppb^{-1}$)							
	This work (k = 2)	Hodnebrog *et al.* (2013)	Hodnebrog *et al.* (2020)	IPCC AR6	Jain *et al.*	Kovac *et al.*	Andersen *et al.*	Li *et al.*
SF_6	0.573 ± 0.016	0.57	0.57	0.567	0.49	0.59		
CF_4	0.085 ± 0.002	0.09	0.10	0.099	0.088			
NF_3	0.195 ± 0.008	0.21	0.20	0.204				
Novec-4710	0.201 ± 0.008						0.223[1)]	
PMVE	0.328 ± 0.013							0.0463
PFMEE	0.544 ± 0.022	No data available						
RF Model	nNBM	hNBM (w/ τ correction)[2)]	nNBM (w/ τ correction)	compilated	NBM	RFM	nNBM	2-D chemical transport
Measurement Range (cm^{-1})	500–3,000	500–2,500	500–3,000	compilated	500–2,500	500–2,000	500–2,500	500–2,500

1) The final value was cited as 0.217 $Wm^{-1}ppb^{-1}$, which was lifetime corrected.
2) τ correction denotes lifetime correction

3.2.2 *Novec-4710*

Among the range of emerging GHGs, *Novec-4710* is considered to be a sustainable replacement for strong gas insulators such as SF_6. Its superior dielectric properties but low GWP are desirable for the insulating materials for eco-friendly GIS (Pan et al., 2020). *Novec-4710* was gravimetrically diluted with a CO_2 broadener to a concentration of 39,967 µmol mol^{-1}. As opposed to the other gases measured, CO_2 was used as the broadener for practical reasons, because a *Novec-4710*/CO_2 mixture has been used in the dielectric medium utilized for the Eco-friendly GIS. Nevertheless, we assumed that the iACS of *Novec*-4710 does not deviate from that obtained when using an N_2 broadener. In general, alien gas broadening is considerably smaller than self-broadening (Johnson et al., 2021). The ACS of *Novec-4710* are shown in Fig. 3. The absorption burden for the ACS measurement of *Novec-4710* was found to be 35.6 cm Torr. Our results revealed that bands in the range of 865–1355 cm^{-1}

https://doi.org/10.5194/acp-2022-667
Preprint. Discussion started: 7 November 2022

Atmospheric Chemistry and Physics Discussions

contributed to almost 90.8% of the RE value, whereas minor bands of 600–785 cm^{-1} contributed an additional 5.1%. Compared with the estimated RE value of 0.217 W m^{-2} ppb^{-1} obtained previously by Andersen et al. using an nNBM model, we obtained a value of 0.201 ± 0.008 W m^{-2} ppb^{-1}, which accordingly implies unresolved uncertainty sources (Andersen et al., 2017). A detailed uncertainty budget for *Novec-4710* is presented in Table 3.

3.2.3 PMVE and PFMEE

PMVE is a new GHG that is used to develop novel fluoroplastics and fluorine rubber, although its climatic impacts have yet to be sufficiently assessed. PMVE was synthesized in our laboratory and broadened by using N_2 as a broadener. Owing to its high flammability, handling with N2 dilution was essential. The absorption burden during the ACS measurement of PMVE was estimated to be 14.8 cm Torr. Li et al. reported that the RE value of PMVE was 0.0499 W m^{-2} ppb^{-1} using a 2-D chemical transport model that evaluated a change in the radiative forcing due to a change in the concentration derived by a modelled vertical decaying profile (Li et al., 2000). The RE value of PMVE estimated with CTMs showed a noticeable underestimation, compared with the present study. The ACS of PMVE obtained in the present study was found to be 1.5 times greater at the strongest band compared with that reported by Li et al., whereas our estimated RE value of 0.328 W m^{-2} ppb^{-1} is 6.8-fold larger than that by Li et al., confirming the underestimation tendency of the 2D CTM model (Li et al., 2000). The significant contribution of RF to PMVE is from the bands within 1135–1365 cm^{-1} (93.1%). An uncertainty budget for PMVE is presented in Table S6.

PFMEE is a prospective substitute for chlorofluorocarbons (CFCs), the absorption burden during the ACS measurement of which was estimated to be 12.4 cm Torr. PFMEE was synthesized in our laboratory and broadened by using N_2 as a broadener. Our findings revealed that bands in the range of 1035–1325 cm^{-1} contributed almost 91.8% to the RE value, and the minor bands at 615–925 cm^{-1} contributed 7.1% to the RE value. The RE value of PFMEE, which we estimated to be 0.544 ± 0.022 W m^{-2} ppb^{-1}, is reported for the first time to the best of our knowledge. Although the overall band shapes of PMVE and PFMEE do not appear to be similarly weighted by the RF model, the ACS intensities of PFMEE at 1000–1500 cm^{-1} were found to be 2-fold higher than those of PMVE, accordingly yielding 2-fold higher RE values. This difference can be attributed to the C=C bonds of PFMEE, which strengthen the structural rigidity to enhance the Franck–Condon overlap integral. The uncertainty budget for PFMEE is presented in Table S7.

https://doi.org/10.5194/acp-2022-667
Preprint. Discussion started: 7 November 2022

Atmospheric Chemistry and Physics Discussions

Table 3. Uncertainty budget for radiative efficiency of *Novec-4710* (representative example, others are presented in the supporting information)

Sources	Symbol	Relative uncertainty (%), k = 1	Sensitivity coefficient	DOF	Distribution	Type	Contribution (%)
OPL of MP[1)]	$ru(L_{MP})$	1.3	-6.3×10^{-4}	∞	Normal	B	38.33
Pressure	$ru(P)$	0.047	-0.071	4	Student's t	A	0.05
Temperature	$ru(T)$	0.194	6.8×10^{-4}	∞	Uniform	A	0.93
Amount fraction	$ru(x)$	1.5	-5.0	∞	Normal	B	55.19
Responsivity drift	$ru(rd)$	0.474	5.2	∞	Normal	B	5.51
Combined uncertainty	$ru(RE)$	2.02		∞	Normal	-	100

1) A detailed budget is provided in the supporting information

4 Conclusion

A RE value for PFMEE, a new GHG, is reported herein for the first time. In addition, we re-evaluated the RE values of NF_3, SF_6, *Novec*-4710, CF_4, and PMVE. Moreover, the utility of a metrology-level measurement of ACSs, performed in conjunction with a direct calibration of L_{MP} mounted in the HR-FTIR spectrometer, is demonstrated for the first time. The RE values of the classic GHGs obtained in this study are consistent with those reported in previous studies, thereby demonstrating the validity of the proposed method. Although the use of different RF models can introduce subtle deviations in the RE values, the proposed method can contribute to reducing the RE uncertainty. The present study establishes measurement traceability to the primary standards for the Beer–Lambert parameters of temperature, pressure, and OPL, which ensure the reliability of the reported RE values. The CC method exhibited a 2.5% uncertainty (at 95% confidence level) for the spectroscopic calibration of the OPL, which contributes approximately 35% to the standard uncertainty of RE. Notably, the dead length within the MP cell is often missed in the product specification, thereby resulting in a systematic error in the evaluation of the OPL (Nwaboh et al., 2014). The CC method was unaffected by the S_T of the referred lines but was sensitive to L_{RC}. Meanwhile, a highly accurate S_T enables the reduction in the $u(L_{MP})$ with a combination of the DLR method, which in addition does not require a COG analysis. Metrological spectroscopic measurements, such as frequency-stabilized cavity ring-down spectroscopy, are a potent tool for establishing line strength with high accuracy (Fleisher et al., 2019).

The second consideration is the significance of the partial pressure of the absorbing gas. As shown in Table 3, the uncertainty in the amount fraction (partial pressure × concentration) contributes approximately 50% to the standard uncertainty of the RE value. Because low-pressure measurements of ACS are required to ensure that no systematic errors have arisen from the saturation effect, using a multipass cell and a pressure broadener is essential. As typical pressure sensor is valid within a dynamic range of 5% to 95%, the pressure added by a broadening agent enhances the accuracy of the pressure reading. However, further improvements in the dilution uncertainty can be achieved by using metrology-level gravimetry (Rhoderick et al., 2014).

https://doi.org/10.5194/acp-2022-667
Preprint. Discussion started: 7 November 2022

Atmospheric Chemistry and Physics Discussions

A third contributing uncertainty source is the responsivity drift of the FTIR spectrometer, which corresponds to a 5% contribution to the standard uncertainty of the RE value. In the quality assurance/quality control process, a high sensitivity coefficient implies that the corresponding measurement parameter should be carefully controlled to improve the measurement quality. Although the sensitivity coefficients of the responsivity drift were 10^4-fold higher than those of OPL calibration, our measurements restricted the corresponding uncertainty well. However, the responsivity drift can be improved by bracketing the I_0 and I measurements.

New GHG substituents and their relevant applications are expected to be actively developed in the coming years, reflecting the continuing drive to replace potent GHGs (e.g., NF_3, SF_6, and CF_4). However, these may have short ALs, and thus high chemical activity. Such compounds should therefore be handled with care by diluting them using inert gases. Hence, we believe the method proposed herein will be beneficial for improving the laboratory measurement procedures for determining RE. In the near future, we intend to extend the measuring window into the far IR range, in which absorption bands contribute approximately 3% to the total RF uncertainty (Hodnebrog et al., 2020).

Data Availability

Data are available at https://doi.org/10.5281/zenodo.7132870 (Beni, 2022)

Supplement

S1. Curve-of-growth measurement for OPL calibration of MP.

S2. Uncertainties in fitted peak area and COG slope.

S3. Parametric evaluation of uncertainty in RE.

Fig. S1. ILS reconstruction results from the N_2O spectrum measurement.

Fig. S2. Responsivity drift measurement.

Table S1. Uncertainty budget of OPL calibration of MP.

Table S2. Referred line data for OPL calibration of MP.

Table S3. Uncertainty budget of RE value of NF_3.

Table S4. Uncertainty budget of RE value of SF_6.

Table S5. Uncertainty budget of RE value of CF_4.

Table S6. Uncertainty budget of RE value of PMVE.

Table S7. Uncertainty budget of RE value of PFMEE.

Author Contributions

Study design: Jeong Sik Lim, Jeongsoon Lee

Methodology establishment: Jeong Sik Lim, Beni Adi Trisna

Measurement: Beni Adi Trisna

Gas synthesis and preparation: Injun Park

Data analysis and uncertainty evaluation: Beni Adi Trisna

Supervision: Jeong Sik Lim, Jeongsson Lee

Validation: Jeong Sik Lim, Jeongsoon Lee, Seungnam Park

Writing – original draft: Jeong Sik Lim, Beni Adi Trisna

Writing – review & editing: Jeong Sik Lim, Beni Adi Trisna

Funding acquisition: Jeong Sik Lim, Jeongsoon Lee

Competing Interests

The authors declare that they have no conflict of interest.

Disclaimer

Publisher's note: Copernicus Publications remains neutral with regard to jurisdictional claims in published maps and institutional affiliations.

Acknowledgments

We thank Dr. Chu-Shik Kang for providing traceability to the standard length measurements. BAT is grateful to Mr. Sangwoo Kim and Ms. Yera Kim for their fruitful discussions and insights.

Financial support

This work was funded by the Korea Research Institute of Standards and Science as a part of a project for establishing measurement standards for climate monitoring based on molecular spectroscopy (22011102). This work was also supported by the Ministry of Trade, Industry and Energy, Republic of Korea, under projects of laser-based radical measurements for the prediction of atmospheric lifetimes of GHGs used in the semiconductor industry (22201050) and GWP 1,000 or Less Chamber Cleaning Gas and its Remote Plasma System for Low GWP Gas (RS-2022-00155753).

References

Allen, M. R., Shine, K. P., Fuglestvedt, J. S., Millar, R. J., Cain, M., Frame, D. J., Macey, A. H.: A solution to the misrepresentations of CO_2-equivalent emissions of short-lived climate pollutants under ambitious mitigation, NPJ Climate and Atmospheric Science, 1, 1-8, https://doi.org/10.1038/s41612-018-0026-8, 2018.

Beni, A. T., Park, S. Park, I. Lee, J. Lim. J. S.: Measurement report: Radiative efficiency estimates of (CF3)2CFCN, CF3OCFCF2, and CF3OCF2CF3 using high-resolution Fourier transform infrared spectroscopy, https://doi.org/10.5281/zenodo.7132870, 2022.

Bravo, I., Aranda, A., Hurley, M. D., Marston, G., Nutt, D. R., Shine, K. P., Smith, K., Wallington, T. J.: Infrared absorption spectra, radiative efficiencies, and global warming potentials of perfluorocarbons: Comparison between experiment and theory, Journal of Geophysical Research Atmospheres, 115, D24317, https://doi.org/10.1029/2010JD014771, 2010.

Denison, S., Forster, P. M., Smith, C. J.: Guidance on emissions metrics for nationally determined contributions under the Paris Agreement, Environmental Research Letter, 14, 124002, https://doi.org/10.1088/1748-9326/ab4df4, 2019.

Fleisher, A. J., Adkins, E. M., Reed, Z. D., Yi, H., Long, D. A., Fleurbaey, H. M., Hodges, J. T.: Twenty-five-fold reduction in measurement uncertainty for a molecular line intensity, Physics Review Letter, 123, 043001, https://doi.org/10.1103/PhysRevLett.123.043001, 2019.

Forster, P. *et al.*: IPCC sixth assessment report (AR6) working group 1: the physical science basis, chapter 7, University Press, UK, www.ipcc.ch/report/ar6/wg1/downloads, 2021.

Gordon, I. E., Rothman, L. S., Hill, C., Kochanov, R. V., Tan, Y., Bernath, P. F., Birk, M., Boudon, V., Campargue, A., Chance, K.: The HITRAN2016 molecular spectroscopic database, Journal of Quantitative Spectroscopy and Radiative Transfer, 203, 3-69, https://doi.org/10.1016/j.jqsrt.2017.06.038, 2017.

Harrison, J. J., Allen, N. D., Bernath, P. F.: Infrared absorption cross sections for ethane (C_2H_6) in the 3 μm region, Journal of Quantitative Spectroscopy and Radiative Transfer, 111, 357-363, https://doi.org/10.1016/j.jqsrt.2009.09.010, 2010.

Harrison, J. J.: Infrared absorption cross sections for 1,1,1,2-tetrafluoroethane, Journal of Quantitative Spectroscopy and Radiative Transfer, 151, 210-216, https://doi.org/10.1016/j.jqsrt.2014.09.023, 2015.

Harrison, J. J.: New infrared absorption cross sections for the infrared limb sounding of sulfur hexafluoride (SF_6), Journal of Quantitative Spectroscopy and Radiative Transfer, 254, 107202, https://doi.org/10.1016/j.jqsrt.2020.107202, 2020.

Hase, F., Blumenstock, T., Paton-Walsh, C.: Analysis of the instrumental line shape of high-resolution Fourier transform IR spectrometers with gas cell measurements and new retrieval software, Applied Optics, 38, 3417-3422, https://doi.org/10.1364/AO.38.003417, 1999.

Hashemi, R., Gordon, I. E., Adkins, E. M., Hodges, J. T., Long, D. A., Birk, M., Loos, J., Boone, C. D., Fleisher, A. J., Predoi-Cross, A., Rothman, L. S.: Improvement of the spectroscopic parameters of the air- and self-broadened NO and CO lines for the HITRAN2020 database applications, Journal of Quantitative Spectroscopy and Radiative Transfer, 271, 107735, https://doi.org/10.1016/j.jqsrt.2021.107735, 2021.

Hodnebrog, Ø., Etminan, M., Fuglestvedt, J. S., Marston, G., Myhre, G., Nielsen, C. J., Shine, K. P., Wallington, T. J.: Global warming potentials and radiative efficiencies of halocarbons and related compounds: A comprehensive review, Review of Geophysics, 51, 300-378, https://doi.org/10.1002/rog.20013, 2013.

Hodnebrog, Ø., Aamaas, B., Fuglestvedt, J. S., Marston, G., Myhre, G., Nielsen, C. J., Sandstad, M., Shine, K. P., Wallington, T. J.: Updated global warming potentials and radiative efficiencies of halocarbons and other weak atmospheric absorbers, Review of Geophysics, 58, e2019RG000691, https://doi.org/10.1029/2019RG000691, 2020.

Hurley, M., Wallington, T., Buchanan, G., Gohar, L., Marston, G., Shine, K.: IR spectrum and radiative forcing of CF_4 revisited, Journal of Geophysical Research Atmospheres, 110, D02102, https://doi.org/10.1029/2004JD005201, 2005.

Jain, A. K., Briegleb, B. P., Minschwaner, K., Wuebbles, D. J.: Radiative forcings and global warming potentials of 39 greenhouse gases, Journal of Geophysical Research Atmospheres, 105, 20773-20790, https://doi.org/10.1029/2000JD900241, 2000.

JCGM 100:2008, Evaluation of measurement data—guide for the expression of uncertainty in measurement, Joint Committee for Guides in Metrology (JCGM/WG1), BIPM, France, https://www.bipm.org/documents/20126/2071204/JCGM_100_2008_E.pdf/cb0ef43f-baa5-11cf-3f85-4dcd86f77bd6, 2008.

https://doi.org/10.5194/acp-2022-667
Preprint. Discussion started: 7 November 2022

Atmospheric Chemistry and Physics Discussions

Johnson, T. J., Hughey, K. D., Blake, T. A., Sharpe, S. W., Myers, T. L., Sams, R. L.: Confirmation of PNNL quantitative infrared cross-sections for isobutane, Journal of Physical Chemistry A, 125, 3793-3801, https://doi.org/10.1021/acs.jpca.1c01933, 2021.

Kim, J. W., Yoo, Y. S., Lee, J. Y., Lee, J. B., Hahn, J. W.: Uncertainty analysis of absolute concentration measurement with continuous-wave cavity ringdown spectroscopy, Applied Optics, 40, 5509-5516, https://doi.org/10.1364/AO.40.005509, 2001.

Kim, J., Lee, J.: Estimation of the global warming potential of fluorinated green house gases, Journal of Korean Society for Atmospheric Environment, 30, 387-397, https://doi.org/10.5572/KOSAE.2014.30.4.387, 2014.

Kovács, T., Feng, W., Totterdill, A., Plane, J., Dhomse, S., Gómez-Martín, J. C., Stiller, G. P., Haenel, F. J., Smith, C., Forster, P. M.: Determination of the atmospheric lifetime and global warming potential of sulfur hexafluoride using a three-dimensional model, Atmospheric Chemistry and Physics, 17, 883-898, https://doi.org/10.5194/acp-17-883-2017, 2017.

Laruelle, E., Kieffel, Y., Ficheux, A.: In international conference on eco-design in electrical engineering, Springer, 139-146, https://link.springer.com/book/10.1007/978-3-319-58172-9, 2017.

Li, Z., Tao, Z., Naik, V., Good, D. A., Hansen, J. C., Jeong, G. R., Francisco, J. S., Jain, A. K., Wuebbles, D. J.: Radiative forcings and global warming potentials of 39 greenhouse gases, Journal of Geophysical Research Atmospheres, 105, 4019-4029, https://doi.org/10.1029/2000JD900241, 2000.

Loos, J., Birk, M., Wagner, G.: Pressure broadening, -shift, speed dependence and line mixing in the v3 rovibrational band of N_2O, Journal of Quantitative Spectroscopy and Radiative Transfer, 151, 300-309, https://doi.org/10.1016/j.jqsrt.2014.10.008, 2015.

Lynch, J., Cain, M., Pierrehumbert, R., Allen, M.: Demonstrating GWP*: a means of reporting warming-equivalent emissions that captures the contrasting impacts of short- and long-lived climate pollutants, Environmental Research Letter, 15, 044023, https://doi.org/10.1088/1748-9326/ab6d7e, 2020.

Nelson, C. T., Overzet, L. J., Goeckner, M. J.: Temperature dependence of the infrared absorption cross-sections of neutral species commonly found in fluorocarbon plasmas, Journal of Vacuum Science & Technology A, 30, 021305, https://doi.org/10.1116/1.3679408, 2012.

Nwaboh, J. A., Witzel, O., Pogány, A., Werhahn, O., Ebert, V.: Optical path length calibration: a standard approach for use in absorption cell-based IR-spectrometric gas analysis, International Journal of Spectroscopy. ID 132607, https://doi.org/10.1155/2014/132607, 2014.

Pagliano, E., Meija, J.: Reducing the matrix effects in chemical analysis: fusion of isotope dilution and standard addition methods, Metrologia, 53, 829-834, https://doi.org/10.1088/0026-1394/53/2/829, 2016.

Pan, B., Wang, G., Shi, H., Shen, J., Ji, H.-K., Kil, G.-S.: Green gas for grid as an eco-friendly alternative insulation gas to SF_6: a review, Applied Science, 10, 2526, https://doi.org/10.3390/app10072526, 2020.

Pinnock, S., Hurley, M. D., Shine, K. P., Wallington, T. J., Smyth, T.: Radiative forcing of climate by hydrochlorofluorocarbons and hydrofluorocarbons, Journal of Geophysical Research Atmospheres, 100, 23227-23238, https://doi.org/10.1029/95JD02323, 1995.

Pinnock, S., Shine, K. P.: The effects of changes in HITRAN and uncertainties in the spectroscopy on infrared irradiance calculations, Journal of Atmospheric Sciences, 55, 1950-1964, https://doi.org/10.1175/1520-0469(1998)055<1950:TEOCIH>2.0.CO;2, 1998.

Rhoderick, G., Guenther, F., Duewer, D., Lee, J., Moon, D., Lee, J., Lim, J. S., Kim, J. S.: Final report on international comparison CCQM-K83: Halocarbons in dry whole air, Metrologia, 51, 08009, https://doi.org/10.1088/0026-1394/51/1A/08009, 2014.

https://doi.org/10.5194/acp-2022-667
Preprint. Discussion started: 7 November 2022

Atmospheric Chemistry and Physics Discussions

Robson, J., Gohar, L., Hurley, M., Shine, K., Wallington, T.: Revised IR spectrum, radiative efficiency and global warming potential of nitrogen trifluoride, Geophysics Research Letter, 33, L10817, https://doi.org/10.1029/2006GL026210, 2006.

Rosenzweig, C., Ruane, A. C., Antle, J., Elliott, J., Ashfaq, M., Chatta, A. A., Ewert, F., Folberth, C., Hathie, I., Havlik, P.: Coordinating AgMIP data and models across global and regional scales for 1.5°C and 2.0°C assessments, Philosophical Transactions of the Royal Society A. 376, 20160455, https://doi.org/10.1098/rsta.2016.0455, 2018.

Shine, K. P., Myhre, G.: The spectral nature of stratospheric temperature adjustment and its application to halocarbon radiative forcing, Journal of Advances in Modeling Earth Systems, 12, e2019MS001951, https://doi.org/10.1029/2019MS001951, 2020.

Smith, T., Wooster, M., Tattaris, M., Griffith, D.: Absolute accuracy and sensitivity analysis of OP-FTIR retrievals of CO_2, CH_4 and CO over concentrations representative of "clean air" and "polluted plumes", Atmospheric Measurement Techniques, 4, 97-116, https://doi.org/10.5194/amt-4-97-2011, 2011.

Sulbaek Andersen, M. P., Kyte, M., Andersen, S. T., Nielsen, C. J., Nielsen, O. J.: Atmospheric chemistry of $(CF_3)_2CF–C{\equiv}N$: a replacement compound for the most potent industrial greenhouse gas, SF_6, Environmental Science and Technology, 51, 1321-1329, https://doi.org/10.1021/acs.est.6b03758, 2017.

Sulbaek Andersen, M. P., Nielsen, O. J., Sherman J. D.: The global warming potentials for anesthetic gas sevoflurane need significant corrections, Environmental Science and Technology, 55, 10189-10191, https://doi.org/10.1021/acs.est.1c02573, 2021.

UNFCCC secretariat: Report of the conference of the parties on its twenty-first session, part two: action taken by the conference of the parties at its twenty-first session, United Nations Framework Convention on Climate Change (UNFCCC), UN: NYC, https://unfccc.int/process-and-meetings/conferences/past-conferences/paris-climate-change-conference-november-2015/cop-21/cop-21-reports, 2015.

Zhao, M., Han, D., Zhou, Z., Zhang, G.: Experimental and theoretical analysis on decomposition and by-product formation process of $(CF_3)_2CFCN$ mixture, AIP Advances. 9, 105204, https://doi.org/10.1063/1.5116211, 2019